Optics and magnetism

Mena, F.P.

Chapter 1

Introduction

Optical spectroscopy is one of the oldest techniques used to determine the properties of materials [1]. Nowadays it is used in an ample variety of fields (e.g. biology, physics, chemistry, astrophysics, materials science, paint restoration, forensics) and materials (e.g. polymers, ferromagnets, organics) in different forms (e.g. solids, liquids, gases). In the work presented in this thesis, optical spectroscopy has been used in different materials of current interest in solid state physics. This introductory chapter describes why optical spectroscopy is important and what can be learnt from it. Furthermore, a brief review of the materials studied in this thesis will be presented. Finally the scope of the present work will be outlined.

1.1 Optical Spectroscopy: Why?

In a dictionary-like definition, it can be said that optical spectroscopy is the use of light to investigate the properties of a material. For the purposes of this work, it has been used to determine the optical conductivity, $\sigma(\omega)$, of the material under study and from there investigate its electronic structure or electronic properties. The question is then, why is optical spectroscopy a good tool to such investigation? To answer this question, I would like to follow A. J. Millis [2] and A. Chattopadhyay et al. [3] who have stated the answer in a simple way. In the first place let us consider the (complex) optical conductivity which simply describes the response of a material to an electric field (for more details see Chapter 2):

$$\boldsymbol{J}(\omega) = \sigma(\omega)\boldsymbol{E}(\omega) \tag{1.1}$$

In other words, the optical conductivity describes how the electrons move in response to an electrical field and, therefore, it can give information about the mechanism associated with this motion. In strongly correlated systems, at low frequencies, the dominant process is the motion from one site to other. This

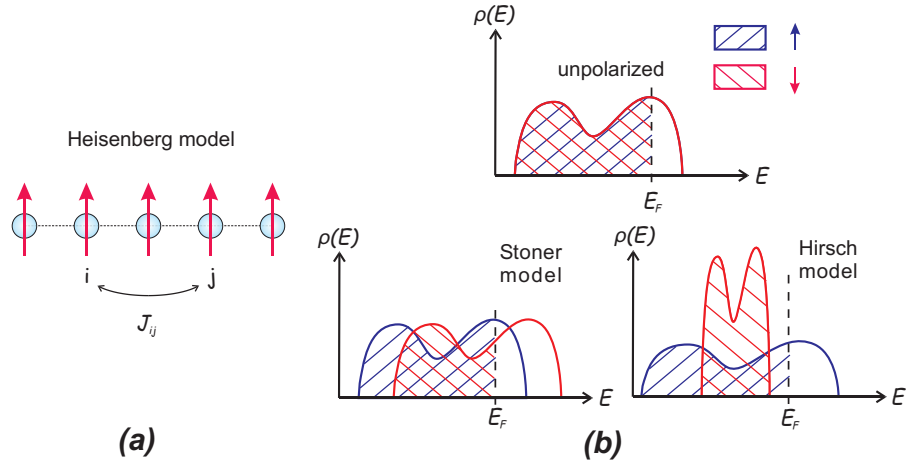

Figure 1.1: *(a) Localized moments: Heisenberg model. (b) Itinerant magnetism: Stoner and Hirsch models (adapted from References [4] and [5]).*

motion is the result of the interplay between repulsive electron-electron interactions (localizing effect) and wave function hybridization (delocalizing effect). This interplay is the essence of strong correlations.

1.2 Magnetism and Strong Correlations

1.2.1 Localized vs. Itinerant Magnetism

The ultimate origin of magnetism in solids is the magnetic moment of their individual atoms (and which originates from the spin and angular momenta of the electron). However, the main question is how this *microscopic* magnetism gives rise to the *macroscopic* magnetism of solids appearing in some materials below a transition temperature, called Curie temperature, T_C. There are two main and opposite streams: localized and itinerant models. The former models start with the electronic states localized in real space, while the latter start with those states localized in reciprocal space [4]. Both situations are schematically represented in Fig. 1.1.

The idea of localized moments is the most intuitive one. It was introduced by Weiss, he argued that the individual magnetic moments interact between them and therefore can align. He represented this interaction by a mean molecular field. Heisenberg attributed this field to the quantum mechanical exchange interaction between neighboring atoms. If $\boldsymbol{S}_i$ is the atomic spin operator at a given site, the

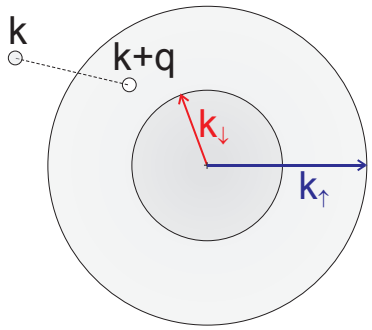

Figure 1.2: *Thermal excitation in a itinerant polarized system (after Ref. [4]). It consists of a spin flip excitation of an electron across the Fermi level. This excitations produce a spin density density fluctuation.*

Heisenberg model for magnetism is:

$$H = \sum_{i,j} J_{ij} \boldsymbol{S}_i \cdot \boldsymbol{S}_j \tag{1.2}$$

where J_{ij} is the interatomic exchange interaction constant. Within this model, the Curie-Weiss law (i.e. $\chi^{-1} \propto T - T_C$, where χ is the magnetic susceptibility) is naturally explained. Moreover, materials considered as having localized moments are expected to have a saturation magnetization, μ_S, which is an integer multiple of the Bohr magneton, μ_B.

On the other hand, magnetism in metals is usually explained from an itinerant picture. One of the main reasons to invoke a different mechanism is that the saturation magnetization, μ_S, is not an integer multiple of μ_B*. In the Stoner model, magnetism in metals arise from a splitting between the up- and down-spin bands and it is favored when the density of states is high at the Fermi level. However, in this form, the Stoner model fails to reproduce the measured T_C and the observed Curie-Weiss law above it. Improvements to this theory have been made that take into account the effect of spin fluctuations (see Fig. 1.2) in a self consistent renormalized (SCR) manner [4]. It is claimed [4] that one of the achievements of SCR theory is the description of several properties of weak itinerant ferromagnets. Several features define this kind of ferromagnets:

a. Low Curie temperature. Usually, less than 50 K.

b. They follow a Curie-Weiss law quite precisely in the temperature interval $T_C < T < 10\ T_C$.

*Other mechanisms involving localized moments can also predict non integer values of μ_S. For example the combination of of spin-orbit interaction and crystal field. Other example is given in Ref. [6] where a Kondo-like mechanism is described and which is responsible for the screening of part of the magnetic moment.

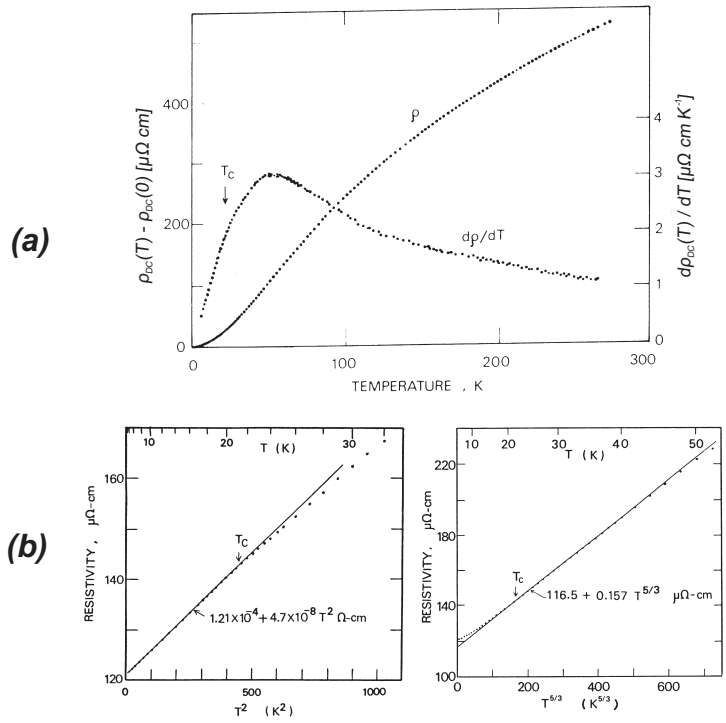

Figure 1.3: *Temperature dependence of ρ_{DC} in $ZrZn_2$. (a) Data from Ref. [8] (b) Analysis by Moriya [4] showing the expected temperature dependencies for spin fluctuations below and above T_C, respectively.*

c. The magnetization inferred from the Curie-Weiss law is several times the saturation magnetization.

It usually appears in materials whose components are not magnetic in elemental form like $ZrZn_2$ and $ScIn_3$. One of the materials studied in this thesis, MnSi, is considered to be well described by the SCR theory. It indeed describes several of its properties like the negative magnetoresistance and the temperature behaviour of the DC resistivity, ρ_{DC}, below T_C (see Fig. 1.3 for the predictions of the SCR theory regarding ρ_{DC}). However, as it will be seen in Chapter 3, the description is not complete. Moreover, other silicides showing itinerant ferromagnetism (Chapter 4) do not follow completely its predictions, namely they show a positive magnetoresistance [7].

More recently, another mechanism for magnetism in itinerant systems has been proposed [5]. This process is sketched in Fig. 1.1. It has been found that magnetism can arise without exchange splitting but with a change in the width of the bands upon spin polarization (although both effects can be combined). The

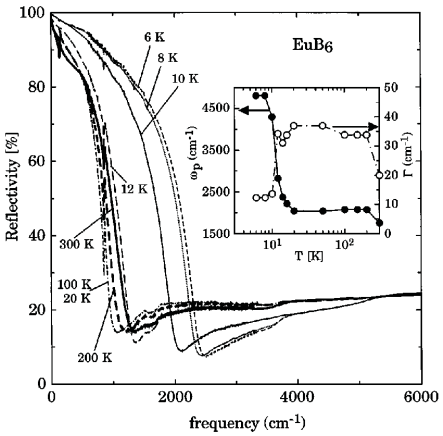

Figure 1.4: *Reflectivity of EuB_6 at several temperatures. The inset shows the temperature dependence of the plasma frequency and width of the Drude peak (from Ref. [11]).*

difference is that ferromagnetism from exchange splitting arises from a gain in potential energy, while in this new model it arises from gain in kinetic energy [5]. This implies that this effect can be seen in optics (see § 1.3). The reduction in kinetic energy produces a transfer of the spectral weight contained in the optical conductivity from high to low frequencies as the system enters to the magnetic state (and vice versa above T_C). Hirsch has argued that this effect could be the driving mechanism in all the different manifestations of metallic ferromagnetism [9]. In fact, optical experiments in manganites (see Chapter 6), manganese doped GaAs [10], and rare earth hexaborides [11] seem to corroborate this point of view. As an example, the optical properties of EuB_6 [11] are shown in Fig. 1.4 where the increase of the spectral weight at low frequencies is manifested by the increase of the plasma frequency of the Drude peak. In contraposition to this trend, it will be seen in Chapters 3 and 4 that the spectral weight at low frequencies decreases when entering the magnetic ordered state in various transition metal silicides.

1.2.2 Heavy Fermion Systems

There are systems where we can find both *kind* of electrons. On one side, there are electrons which are localized and are responsible for the magnetic properties. On the other side, electrons which are delocalized and are responsible for the transport properties. If they interact it gives rise to a multitude of interesting phenomena. One of such systems are the so-called heavy fermion systems. Heavy fermion systems are compounds which usually have an atom (e.g. Ce or U) containing well localized $4f$ or $5f$ electrons.[†] Below a characteristic temperature T^* heavy

[†]Recently some compounds have appeared which only contain d electrons (e.g. LiV_2O_4 [12]) that have similar properties as the heavy fermion compounds. Whether they are also governed

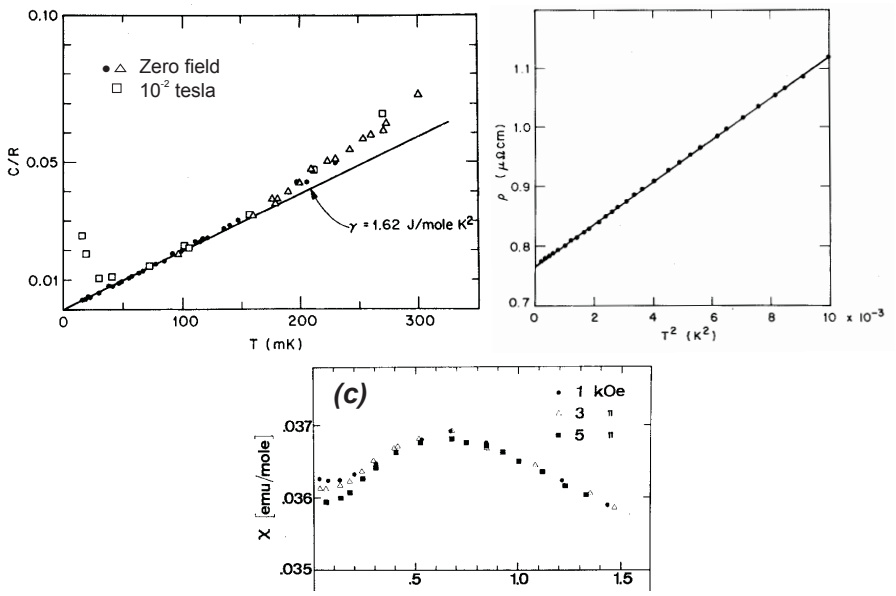

Figure 1.5: *(a) Specific heat, (b) resistivity, and magnetic susceptibility in the first heavy fermion metal discovered, $CeAl_3$ [15].*

fermion systems show a Fermi-liquid behaviour with large effective masses, m^*, of the quasiparticles. In fact, the physical quantities describing the system have the same temperature dependencies as the normal metals but with much larger proportional constants and at lower temperatures. [13, 14]

Three conditions are usually taken as defining a heavy fermion system at low temperatures[‡]:

a. The specific heat is linear with temperature, $C = \gamma T$;

b. The magnetic susceptibility, χ, is constant (Pauli like);

c. The Wilson's ratio, $R_W = \frac{\pi^2 k_B^2 \chi}{3\mu_{eff}^2 \gamma}$, is of order unity ($\mu_{eff}$ is the effective moment of the quasiparticles).

Since γ and χ are proportional to $N(0)$ which, in turn, is proportional to the effective mass of the fermionic excitations, m^*, their large values can be interpreted

by the same physical process is an ongoing debate.

[‡]Remember that for a Fermi gas the specific heat and the susceptibility at low temperatures are given, respectively, by [16]: $C = \frac{1}{3}\pi^2 N(0) k_B^2 T$, and $\chi = N(0)\mu^2$, where $N(0)$ is the density of states at the Fermi level and μ is the magnetic moment of the electron

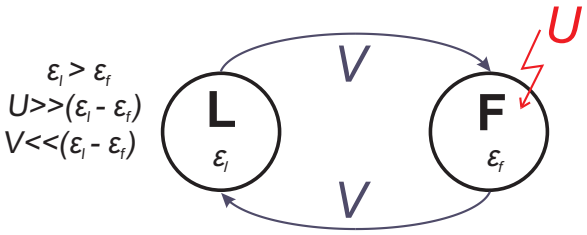

Figure 1.6: *Simplest example of a strongly correlated system (after Ref. [13]). The system contains two orbitals denoted L and F with energies ε_L and ε_F, respectively. Between them, there is an hybridization V. Putting two electrons in the orbital F costs an energy U. Electron interactions in the orbital L and between the two orbitals are neglected.*

as an enhancement of the mass of the quasiparticles. If conditions a.-c. are met, it is possible to say that there is a one-to-one correspondence between the quasiparticle excitations in this system and those in a Fermi gas. Other quantities behave also as in normal metals, e.g. the DC resistivity which is proportional to T^2. As an example consider Fig. 1.5 where C, χ and ρ_{DC} of $CeAl_3$ are plotted [15]. If $R \neq 1$ the interaction between quasiparticles is also important. When $T > T^*$, the excitations lose their heavy fermion character: the specific heat levels off and the susceptibility changes from Pauli- to Curie-like. In the remainder of this subsection, the mechanism originating this behaviour is sketched.

A Strongly Correlated Molecule

Following Fulde [13], let us first consider the system depicted in Fig. 1.6 which contains the main ingredients necessary to understand the heavy fermion systems. The Hamiltonian describing it is:

$$H = \varepsilon_l \sum_\sigma l_\sigma^\dagger l_\sigma + \varepsilon_f \sum_\sigma f_\sigma^\dagger f_\sigma + V \sum_\sigma \left(l_\sigma^\dagger f_\sigma + f_\sigma^\dagger l_\sigma \right) + U n_\uparrow^f n_\downarrow^f \tag{1.3}$$

each term describes, respectively, kinetic energy in orbital L, kinetic energy in orbital F, hybridization between the two orbitals, and electron interaction in orbital F. For $V = 0$ and $V \neq 0$ the accessible states and their are sketched in Fig. 1.7. In the former case, the ground state is 4-fold degenerate (one electron in L and the other in F, therefore forming a singlet and a triplet states) and there is one excited level[§] (two electrons in L). If the hybridization is turned on, the degeneracy of the ground state is partially lifted since now the singlet and the excited states are coupled. The singlet lowers its energy by $2V^2/\Delta\varepsilon$ while the excited state increases its energy by the same amount. The occupancy of F, in this case, is $n_f = 1 - 2(V^2/\Delta\varepsilon)^2 < 1$.

[§]There is another excited state (2 electrons in F) not considered due to the large value of U

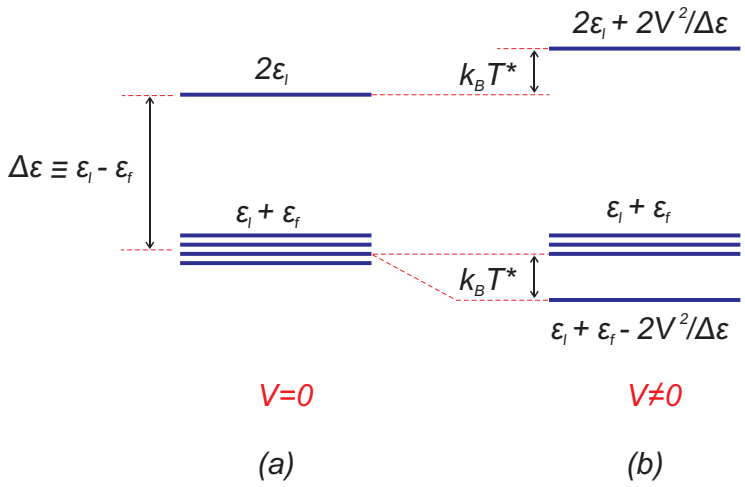

Figure 1.7: *Accessible states and energies in the system considered in Fig. 1.6 for (a) $V = 0$ and (b) $V \neq 0$.*

The system, thus, has a characteristic temperature $T^* \equiv 2V^2/\Delta\varepsilon$. At $T \ll T^*$ we can distinguish two different kind of excitations:

a. low-lying spin excitations (between the singlet and triplet states), with an energy $k_B T$;

b. excitations involving charge degrees of freedom (promotion of an f electron into the ligand orbital), with an excitation energy $\Delta\varepsilon$.

The basic ingredients of this system are the following. At $T = 0$, the ground state is a singlet and the moment of the partially filled F state is zero. When the temperature increases, with $T \ll T^*$, the triplet state starts to be populated. Since the triplet has a moment, the magnetic moment of the f electron starts to appear. For $T \gg T^*$, the magnetic moment is fully present and the singlet character of the ground state is not noticeable.

Kondo Problem: A Single Magnetic Impurity

Now, let us consider the case of a magnetic impurity, e.g. Ce, embedded in a metal. This impurity has a total moment $\boldsymbol{j}$ whose z component is described by the quantum number m. Then the Hamiltonian describing the system is:

$$\begin{aligned} H &= \sum_{\mathbf{k}\sigma} \varepsilon(\mathbf{k}) c^\dagger_{\mathbf{k}\sigma} c_{\mathbf{k}\sigma} + \varepsilon_f \sum_m f^\dagger_m f_m \\ &\quad + \sum_{\mathbf{k}m\sigma} \left[V^*_{m\sigma}(\mathbf{k}) c^\dagger_{\mathbf{k}\sigma} f_m + V_{m\sigma}(\mathbf{k}) f^\dagger_m c_{\mathbf{k}\sigma} \right] + \tfrac{U}{2} \sum_{m \neq m'} n^f_m n^f_{m'} \end{aligned} \tag{1.4}$$

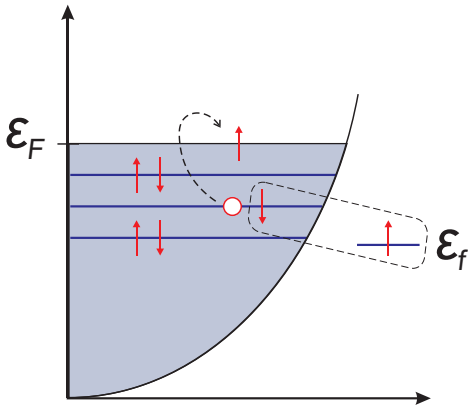

Figure 1.8: *Single magnetic impurity embedded in a metal. After one of the conduction electrons is moved to the Fermi level, the resulting system is similar to the one depicted in Fig. 1.6. The f impurity can form a singlet with the conduction electron which lost its companying electron.*

where, similarly as before, the terms represent the kinetic energy of the conduction electrons (which now form a band), the kinetic energy of the f-electrons (now the f orbital is ν_f-fold degenerate), the hybridization between conduction electrons and the f-electrons, and the electron repulsion between f-electrons, respectively. The situation for $\nu_f = 2$ is represented in Fig. 1.8. If one of the conduction electrons is promoted to the Fermi level, the situation is similar to the one described above for the $L-F$ system. The remaining conduction electron can form a singlet with the f-electron. The difference with the $L-F$ system is that the singlet formation can occur with different conduction-electron states. Those which are closer to ε_F are more important since for them it is easier to promote an electron to the Fermi level. It results that, in the $U \to \infty$ limit and in the presence of weak hybridization, the energy of the singlet state is always lower that the energy of the multiplets, just as in the case presented above. The lowering of the energy due to hybridization is (for details of the calculation see [13]):

$$\varepsilon = -D\,\mathrm{e}^{-|\varepsilon_f|/(\nu_f N(0) V^2)}$$

where a constant density of states is assumed with height $N(0)$ and a lower cutoff D. To this energy it is customary to associate a characteristic temperature T_K (Kondo temperature), $k_B T_K = -\varepsilon$. At $T \ll T_K$ we find again the two kind of excitations characteristic of strongly correlated systems.

The Kondo Lattice

Finally, let us consider an array of magnetic atoms (which is the case of heavy fermion systems). The respective Hamiltonian can be obtained by generalizing

Eq. 1.4:

$$\begin{aligned} H &= \sum_{\mathbf{k}n\sigma} \varepsilon_n(\mathbf{k}) a^\dagger_{\mathbf{k}n\sigma} a_{\mathbf{k}n\sigma} + \sum_{mi} \varepsilon_{fm} f^\dagger_m(i) f_m(i) \\ &+ \tfrac{1}{\sqrt{N_o}} \sum_{im\mathbf{k}n\sigma} V_{m\sigma}(\mathbf{k}, n) \left[a^\dagger_{\mathbf{k}n\sigma} f_m(i) \mathrm{e}^{-\mathrm{i}\mathbf{k}\cdot\mathbf{R_i}} + f^\dagger_m(i) a_{\mathbf{k}n\sigma} \mathrm{e}^{\mathrm{i}\mathbf{k}\cdot\mathbf{R_i}} \right] \\ &+ \tfrac{U}{2} \sum_{i, m\neq m'} n^f_m(i) n^f_{m'}(i) \end{aligned} \quad (1.5)$$

where i labels the N_o f-sites at positions $\mathbf{R_i}$, and n is a band index. In the limit $U \to \infty$, the previous Hamiltonian can be solved using a mean field approximation [13, 17] where it is assumed that the strong repulsion between the f electrons can be taken into account by a renormalization of the hybridization matrix element $V_{m\sigma}(\mathbf{k}, n) \to r V_{m\sigma}(\mathbf{k}, n) = \tilde{V}_{m\sigma}(\mathbf{k}, n)$. With this method, we can map the many-body problem (Eq. 1.5) into a one-particle problem:

$$H_{MF} = \sum_{\mathbf{k}l\tau} E_l(\mathbf{k}) c^\dagger_{l\tau}(\mathbf{k}) c_{l\tau}(\mathbf{k}) + \Lambda N_o (r^2 - 1)$$

where $c^\dagger_{l\tau}(\mathbf{k})$ denotes the creation operators of quasiparticles in branch l with pseudospin τ, and Λ is a Lagrange parameter. For the case of one conduction electron band and an f orbital degeneracy $\nu_f = 2$ (so the index m is not necessary), at $T = 0$, two quasiparticle bands are found:

$$E_l(\mathbf{k}) = \frac{1}{2} \left\{ [\varepsilon(\mathbf{k}) + \tilde{\varepsilon}_f] \mp W(\varepsilon(\mathbf{k})) \right\} \quad (1.6)$$

where $W(\varepsilon(\mathbf{k})) = \sqrt{[\varepsilon(\mathbf{k}) + \tilde{\varepsilon}_f]^2 + 4\tilde{V}^2}$, and $\tilde{\varepsilon}_f = \mu + \frac{\tilde{V}^2}{\varepsilon(k_F) - \mu}$ if the condition $E_l(k_F) = \mu$ is applied (μ is the chemical potential). This situation is depicted in Fig. 1.9.

The unknowns r and Λ can be expressed in terms of the system parameters. In particular, it is found that $\Lambda = \nu_f N(0) V^2 \ln\left(\frac{[\varepsilon(k_F) - \mu]\mu}{\tilde{V}^2} \right)$ which permits defining a characteristic temperature:

$$k_B T^* \equiv \mu \, \mathrm{e}^{-\frac{\Lambda}{\nu_f N(0) V^2}} \quad (1.7)$$

With this definition, we obtain $\tilde{\varepsilon}_f = \mu + k_B T^*$. The characteristic temperature T^* is related to the energy gain of the system due to hybridization. In fact it can be shown that the difference between the hybridized system, E, and the energy without hybridization, $E^{(0)}$, is

$$E - E^{(0)} = -k_B T^*$$

The temperature T^* plays the role of a Kondo temperature for the lattice (they are not the same and usually $T^* < T_K$). Calculations at finite temperatures show that there exists a critical temperature of the order of T^* below which there exist

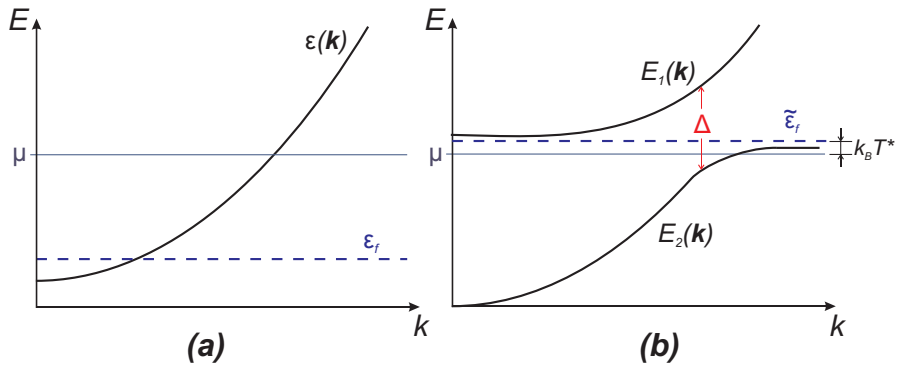

Figure 1.9: *Schematic representation of the hybridization gap (adapted from References [13] and [17]) (a) At high temperatures ($T \gg T^*$), in the Kondo lattice, the conduction electrons and the magnetic moments are independent. (b) At low temperatures ($T \ll T^*$), both set of electrons hybridize, and the system can be represented as renormalized quasiparticles which occupy two bands. If the Fermi energy lies within the lower band, the system is a heavy fermion metal.*

solutions to the problem with $r \neq 0$. Above this critical temperature, it is found that $r = 0$ and the conduction electrons are completely decoupled from the f electrons.

As we have seen, the origin of the heavy fermion behaviour in a Kondo lattice is the weak hybridization between the f electrons with the electrons of neighboring atoms. As in the case of the single impurity problem, there are two different kind of excitations:

a. Low-energy singlet-triplet excitations associated with each f site. A direct evidence of this is the large quasiparticle density of states inferred from the large specific heat (i.e. the f electrons are seemingly located right at the Fermi energy).

b. High-energy excitations involving charge degrees of freedom. This is evinced in photoemission experiments where it takes 2 eV to promote an f electron into an unoccupied conduction electron state above the Fermi energy, in apparent contradiction to the f electrons seemingly located right at ε_F.

As we will see in Chapter 5, with optical spectroscopy it is possible to see both kind of excitations. In particular, the low-energy optical response is a direct consequence of the band structure renormalization depicted in Fig. 1.9.

Because the f sites form a lattice, the excitations are coupled to each other. Below certain temperature T_{coh} (such that $T_{coh} < T^*$), they form coherent quasiparticle states with large effective masses (which are seen in the specific heat, for example). T_{coh} can be approximately determined by measuring the temperature

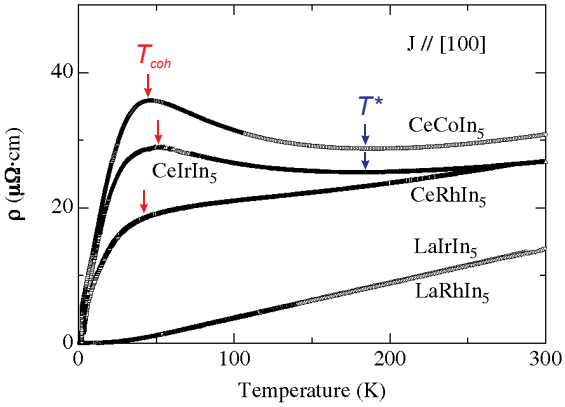

Figure 1.10: *DC resistivity of the heavy fermion compounds studied in Chapter 5 (from [18]). The arrows indicate T_{coh} and T^*, respectively. In these compounds, however, below T_{coh} the resistivity is linear with temperature indicating a non-conventional formation of the coherent state. Moreover, $CeRhIn_5$ does not show the typical behavior of a heavy fermion system. One reason of the reasons is that this compound orders antiferromagnetically below 4 K. The figure also shows the resistivity of two of the relative compounds not containing f electrons.*

dependence of the DC resistivity (see Fig. 1.10). Starting from high temperatures (usually room temperature), ρ_{DC} decreases with decreasing temperature until it reaches a minimum associated with T^*, from there ρ_{DC} increases (this behavior is similar to the one found in the single impurity system). However, in contrast to the the single impurity problem, ρ_{DC} in the lattice reaches a maximum (labeled as T_{coh}). Below T_{coh}, the resistivity decreases due to the formation of coherent Bloch-like states, and $\rho_{DC} = AT^2$ is observed, typical of electron-electron correlations.

For $T > T_{coh}$, the mean-free path of the excitations of the f electron system becomes so short that the coherence starts to be destroyed and the heavy quasiparticles start to disappear. For $T_{coh} \ll T^*$, the specific heat contains contributions of both the coherent and incoherent part of the f electron excitations. Finally, when $T \gg T^*$, the f electrons can be treated as localized and interacting weakly with the conduction electrons.

1.2.3 Manganites

The phase diagram of the perovskite manganites of the general composition $Re_{1-x}A_xMnO_3$ (Re = rare earth, A = divalent alkali) is extremely rich. For example, see Fig. 1.11 where the phase diagram of one of the best studied manganite system compounds, $La_{1-x}Ca_xMnO_3$, is shown [19]. The origin of this

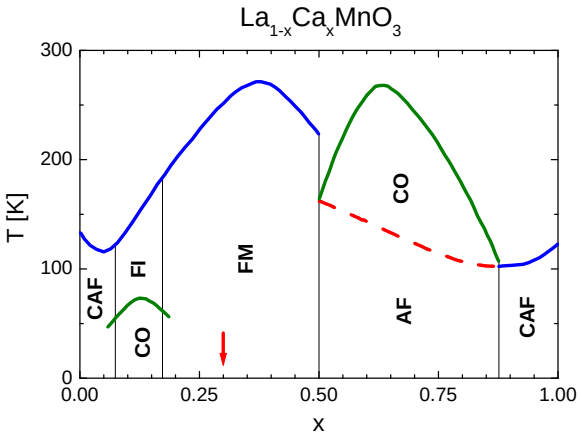

Figure 1.11: *Phase diagram of $La_{1-x}Ca_xMnO_3$ (from Ref. [19]). The richness of this phase diagram is evident, it comprise the following states: canted antiferromagnet (CAF), charge order (CO), ferromagnetic insulator (FI), ferromagnet(FM), and antiferromagnet (AF). The arrow indicates the parent compound of the manganites studied in Chapter 6.*

behaviour is also the interrelation between localized and itinerant electrons as we will see below. The difference is that in this case, both electrons pertain to the same class of atoms.

The basic crystal structure of the manganites is shown in Fig. 1.12. The main point here is that the Mn ion is surrounded by O atoms forming an octahedron. In a perfect octahedron, the crystal field leaves partially the degeneracy of the d levels forming a triple degenerate, t_{2g}, and a double degenerate, e_g, states. The distortions usually present in the octahedron alters this splitting depending on whether the e_g level is occupied or not (see Fig. 1.12). When it is occupied, the e_g level is further split (Jahn-Teller splitting), otherwise this level decreases its energy if it is occupied in a short time scale (like in optical transitions) compared to the response of the lattice. Let us consider the two extremes of the phase diagram of Fig. 1.11. $CaMnO_3$ has the ionic composition $Ca^{+2}Mn^{+4}O_2^{-2}$ [20]. Therefore, the manganese atom has three electrons occupying the t_{2g} level that, due to the strong Hund's coupling, J_H, form a large (classical) spin, $\boldsymbol{S}$. These classical spins tend to align antiferromagnetically between them. On the other hand, in $LaMnO_3$ manganese is present as Mn^{+3} and, therefore, has an itinerant electron occupying the e_g level that tends to align with the spin of the t_{2g} core due to J_H. Between these two extremes, both Mn ions are present in the ratio $Mn^{+3}/Mn^{+4} = x$. The situation described is known as the *double exchange* mechanism and was already proposed by Zener [20] in the fifties just after the discovery of the interesting

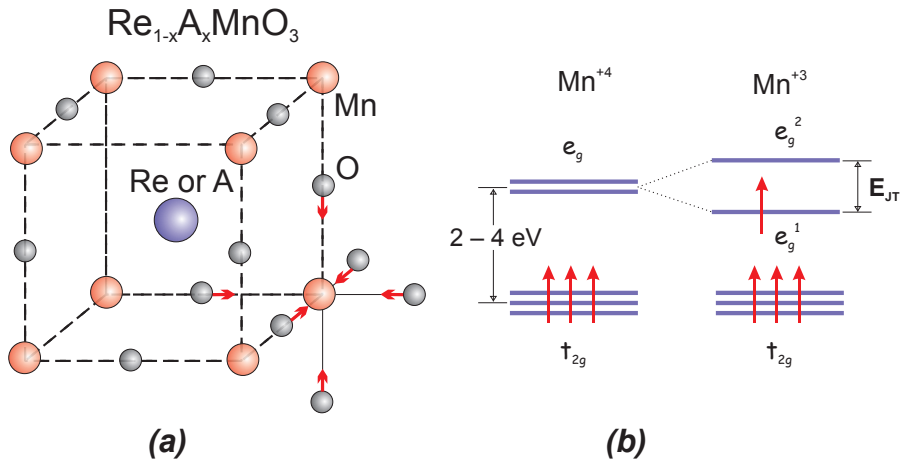

Figure 1.12: *(a) Basic crystal structure of the manganites. One of the main important points to notice is the octahedral surrounding of the Mn atoms. (b) In a perfect environment, its degenerate d levels are split in the triple degenerate t_{2g} and double degenerate e_g. A distortion of the octahedron, like the one indicated by arrows, alters this situation depending on whether the e_g level is occupied or not. If e_g is occupied, it is further split. If not, the e_g level can lower its energy if it is occupied in a short time scale [19].*

properties of the manganites [21]. The double exchange (DE) Hamiltonian is:

$$H = -t \sum_{\langle ij \rangle} c^{\dagger}_{i\sigma} c_{j\sigma} + J \sum_{\langle ij \rangle} \boldsymbol{S}_i \boldsymbol{S}_j - J_H \sum \boldsymbol{S}_i c^{\dagger}_{i\sigma} \boldsymbol{\sigma} c_{i\sigma} \tag{1.8}$$

There are no doubts that the DE Hamiltonian contains the most important physics describing the manganites, especially in describing, at least qualitatively, the ferromagnetic state. However, another mechanism and ideas have to be added for a complete description, although to what extent is still matter of discussion [22]. The most notorious are electron-lattice coupling [19] and phase segregation [23]. Besides the electron-lattice coupling described above (lattice distortions producing modifications in the electron configuration), there is another type called *tolerance factor* [19]. It originates from the fact that the atoms Re and A, in $Re_{1-x}A_xMnO_3$, have different radiuses producing different stresses in the Mn-O-Mn bonds. This, in turn, produces buckling of the MnO_6 octahedron, which changes the Mn-Mn electron hoping [24]. Electron-phonon coupling makes the carriers have a tendency to *self trapping*: the presence of an electron in a given Mn orbital disturbs the lattice which in turn produce a potential minimum that tend to keep the electron in that orbital [19]. If the coupling is strong enough a self trapped state, called *polaron*, can be formed. Polaron states, indeed, have been seen in the optical spectra of manganites. Other indication given by optics

regarding the importance of lattice distortions is the different spectra obtained in cleaved and polished samples. These two points will be discussed in Chapter 6. There, we will also discuss the large isotope effect in some manganites that also point to the importance to electron-phonon coupling.

The other idea that has to be included in describing the manganites is phase separation. The traditional treatment of Eq. 1.8 for $J_H \gg t > J$ concludes that hole doping (increasing x) of the AF state produces a canting of the spins until a certain crital concentration is reached where the material becomes FM [25]. However, from the same treatment it is found that the compressibility $\partial^2 E/\partial^2 x < 0$, where E is the electron energy [26]. This means that the canted phase is unstable and tends to phase separate. The same conclusion has been found by numerical calculations [27, 28] and more elaborate treatments of the DE Hamiltonian [28, 29]. In particular, in Ref. [28] it was found a phase diagram similar to the one found in the traditional treatment [25] with the difference that the canted phase was replaced by a region with phase separation. The phase separated phases, however, will not be large as Coulomb repulsion tends to homogenize the system [26, 23]. In Chapter 6 we will see that the optical data in $(La_{0.5}Pr_{0.5})_{0.7}Ca_{0.3}MnO_3$ thin films can also be interpreted in terms of phase separation.

1.3 Spectral Weight and Strong Correlations

One quantity that we will study in this thesis is the spectral weight contained in the optical conductivity. As we will see in this section, it contains information about strong correlations present in a a given material. Starting from the Kubo formula, it has been demonstrated [30, 31] that the real part of the optical conductivity complies with:

$$\int_0^\infty \sigma_1(\omega)\mathrm{d}\omega = -\frac{1}{2\hbar}\pi \mathrm{i} V \langle [\mathcal{P}, \mathcal{J}] \rangle \tag{1.9}$$

where V is the total volume and $\mathcal{P}$ and $\mathcal{J}$ are the polarization and current density operators, respectively. The important point is that if *all electrons and all bands* are included [32] the current and polarization operators are given by:

$$\begin{aligned} \mathcal{J} &= \frac{e}{Vm}\sum_i p_i\, \delta(r - r_i) \\ \mathcal{P} &= \frac{e}{V}\sum_i r_i\, \delta(r - r_i) \end{aligned}$$

With these relations, Eq. 1.9 can be written as:

$$\int_0^\infty \sigma_1(\omega)\mathrm{d}\omega = \frac{\pi n e^2}{2m} \tag{1.10}$$

where $n \equiv N/V$. This expression is, evidently, temperature independent.

Now, in strongly correlated systems the electronic states of interest seem to be located in narrow bands well separated from other bands [2]. Therefore, tight binding models considering only few bands, such as the Hubbard and Anderson hamiltonians, are used to describe these systems. Within these models, if only nearest neighbor hopping is considered and the system has orthorombic symmetry, the current and polarization operators in a given direction are (for simplicity, summations in the spin degree of freedom are omitted)[31]:

$$\begin{aligned} \mathcal{J} &= \mathrm{i}\frac{eat}{\hbar V}\sum_i \left(c_{i+1}^\dagger c_i - c_i^\dagger c_{i+1}\right) \\ \mathcal{P} &= \frac{ea}{V}\sum_i i c_i^\dagger c_i \end{aligned}$$

where a is the distance between neighboring sites in the considered direction and t is the hopping parameter. Then, Eq. 1.9 can be written as [31]:

$$\int_0^\infty \sigma_1(\omega)\mathrm{d}\omega = -\frac{\pi n e^2 a^2}{2\hbar^2}\langle K\rangle \tag{1.11}$$

where $K = -t\sum_i (c_i^\dagger c_{i+1} + c_{i+1}^\dagger c_i)$ is the kinetic energy of the conduction electrons. The kinetic energy depends on temperature and interaction strength. Therefore, the integrated optical conductivity contain information about the interactions [2]. Moreover, it will have a strong temperature dependence. Equation 1.11 also implies that there should be a transfer of spectral weight to high frequencies, i.e. to energies corresponding to the bands that were not included in the model [32].

In the following chapters we will see that in strongly correlated systems there is, indeed, a large transfer of spectral weight between low to high energies. The range were this transfer occurs depends on the bands involved. In the systems containing d electrons (silicides and manganites), this range is much larger than those involving f electrons (heavy fermion systems).

1.4 Scope of This Thesis

This thesis will start with a short review of the basic concepts of optical spectroscopy, as well as of the experimental techniques used (Chapter 2). The following two Chapters deal with the optical properties of several transition-metal monosilicides. In Chapter 3 one of them, MnSi, is studied thoroughly. Although it is considered as a typical example of a weak ferromagnet described by the SCR theory, it will be seen that is not the case. Particular emphasis will be given to the low frequency properties studied by means of a not so often used optical technique, grazing incidence reflectivity. Chapter 4 studies FeSi, CoSi, and some solid solutions between them. FeSi is a system that has been studied for a relatively

long time. It is not clear if the insulating non-magnetic ground state should be described by an itinerant or a Kondo-like picture. By studying the transferred spectral weight it will be argued that the latter is more appropriate. Although CoSi, as FeSi, is not magnetic, solid solutions between them present, surprisingly, magnetism. Their optical properties are different from other well studied magnetic materials. After studying these itinerant systems, a family of heavy fermion systems ($CeMIn_5$) will be studied in Chapter 5. In this material it is clear that there exist itinerant and localized electrons. The interaction between them gives rise to the heavy fermion behaviour at low temperatures. The formation of this *condensate* is characterized by a hybridization gap which is pretty clear in the optical response. As in the silicides, there is a transfer of spectral weight but the region where it occurs is much smaller. Finally, another system containing localized and itinerant electrons will be studied. Chapter 6 present the optical properties of $(La_{1-y}Pr_y)_{0.7}Ca_{0.3}MnO_3$ ($y = 0.5$) thin films. Phase separation and transfer of spectral weight will be analyzed. Moreover, a comparison between films containing different oxygen isotopes will be made.